Journal of the Korean Physical Society, Vol. 74, No. 8, April 2019, pp. 779∼784

Single Remote-Sensing Image Dehazing in HSI Color Space

Yongfei Guo, Zeshu Zhang and Hangfei Yuan
Changchun Institute of Optics, Fine Mechanics and Physics, Chinese Academy of Sciences, Changchun 130033, China

Shuai Shao*
Changchun Institute of Optics, Fine Mechanics and Physics, Chinese Academy of Sciences, Changchun 130033, China and University of Chinese Academy of Sciences, Beijing 100049, China

(Received 21 November 2018, in final form 26 December 2018)

In order to improve the visibility of a single hazy remote sensing multi-spectral image, we develop a novel and effective dehazing algorithm in HSI (hue, saturation and intensity) color space. First of all, the hazy image is transformed into HSI color space; then a linear regression model is built for saturation component image processing. In addition, we implement the improved dark channel prior method in the intensity channel processing. Compared with the traditional haze removal methods in remote-sensing images, the experimental results demonstrate that the developed algorithm can achieve better visual effect and better color fidelity. Both qualitative evaluations and quantitative assessments indicate that the proposed method achieves a better performance than the state-of-the-art methods.

PACS numbers: 42.30.−d, 42.30.Tz, 42.30.Va, 42.40.My
Keywords: Remote-sensing image, HSI color space, Haze removal, Linear regression model
DOI: 10.3938/jkps.74.779

I. INTRODUCTION

The rapid development of computer technology and remote-sensing techniques has brought new opportunities for the application of remote-sensing image processing. The images are widely used in basic geographic information acquisition, agricultural production, marine monitoring and other fields because of their wide coverage and high resolution [1–3]. Nearly all images acquired by passive optical remote sensing are disturbed by clouds, fog, haze and other weather factors, resulting in light being absorbed and scattered by turbid media such as particles and water droplets in the atmosphere [4–6]. The removal of haze from a single remote-sensing image is still a significant task.

At present, dehazing methods can be divided into two main categories. The first is methods based on image enhancement; the second is based on physical models. Methods in first category enhance degraded images and improve quality, and existing mature image processing algorithms can be applied to haze removal. However, the method in this category may result in some information in the images being lost. The histogram equalization method, which is based on the gray-level cumulative distribution function of the image, can also be used for dehazing, The essence of histogram equalization is the non-linear stretching of an image to enhance contrast [7–9]. In foggy weather, the low-frequency component of the image is enhanced, so a high-pass filter can be used to filter the image to suppress the low-frequency and enhance the high-frequency. At present, holomorphic filtering is being widely studied to remove haze [10]. According to Retinex theory, if we can find a way to separate the reflected component from the image, then the effect of the incident component on the image is reduced to enhance the image. In the development of Retinex theory, the path-based Retinex algorithm and the iterative Retinex algorithm have appeared successively. These algorithms are highly complex, and adjusting their parameters are difficult [11,12].

The second category includes the atmospheric scattering model based on the research of the atmospheric suspended-particles scattering-effect on light. This is a special method for image restoration and has a good effect on complex-scene image processing. Therefore, the information in the image can be preserved completely and haze can be removed. Tan [13] first proposed a single image-dehazing method by maximizing the local contrast of the image. However, Tan's proposed method can easily cause color over saturation when processing dense haze images. He *et al.* [14] summarized a rule, called the

*E-mail: damond0424@yeah.net

dark channel prior (DCP) based on observing the statistical characteristics pertaining to a large number of haze-free images. Among the above dehazing methods, He's method is simple and effective. However, the DCP methods are based on the statistics of outdoor images while remote-sensing images have an imaging distance different from outdoor images. As a result, color drift can easily occur when that method is applied to remote-sensing images.

In this paper, we propose a novel haze-removal method for a single hazy remote-sensing image. In order to remove the haze and maintain the color information of the original image better, we transform the hazy image into HSI color space; then, we build a linear regression model for saturation component image processing. In addition, we implement the improved DCP method in the intensity channel processing. Compared with the traditional methods for removing haze from remote-sensing hazy images, the proposed method achieves better visual effect in color fidelity and haze removal.

II. METHODOLOGY

1. The physical hazy image degradation model

Nayer *et al.* [15,16] described and deduced in detail the atmospheric scattering model, which was widely referred to by later researchers. In that model, the effect of atmosphere on the light reflected from scenery is divided into two parts: the attenuation by the atmosphere of light the scenery and the superposition of environment light. Attenuation refers to light reflected by the scene reaching to the observer after having been scattered by atmospheric particles. The image degradation model is expressed in RGB space as follows:

$$\mathbf{I}(x) = \mathbf{J}(x)t(x) + \mathbf{A}(1 - t\,(x))\,, \tag{1}$$

where x represents the position of the pixel in the image, $\mathbf{I}(x)$ is the intensity of the observed hazy image, $\mathbf{J}(x)$ is the scene radiance, $\mathbf{A}$ is the global atmospheric light which is usually assumed to be constant, and $t(x)$ is the medium transmission, which describes the fraction of the light that is not scattered and gets to the camera.

2. Color space conversion

The main purpose of the RGB color space is for the representation and display of images in electronic systems, such as televisions and computers. The color information collected from the pixels by common devices is stored by dividing it into R (red), G (green) and B (blue). However, in RGB color model, the chrominance information is vulnerable to brightness [16].

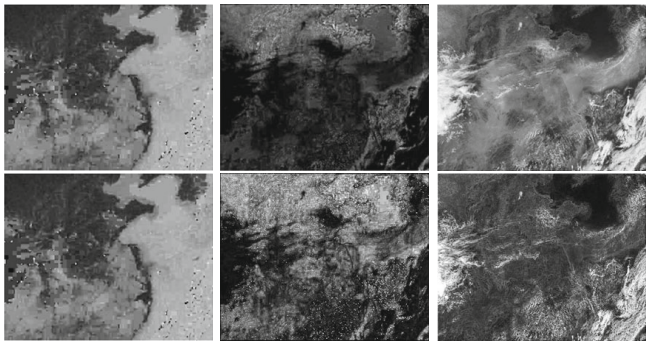

(a) Hue component image (b) Saturation component image (c) Intensity component image

Fig. 1. Comparison of the H, S, and I image components before and after haze removal. The top row shown hazy images images, and the bottom row shown the haze-free images.

The existence of haze submerges the object's light in the intensity channel, which could lead to a low contrast image. What's more, the saturation component is slightly affected due to the different scattering coefficients, which will be discussed in next section. When people observe objects, they tend to describe them in terms of hue, saturation and brightness (HSI). HSI color space is widely used in computer vision processing algorithms, and the HSI model is more suitable for the subjective description and interpretation of the human eyes. The image is divided into a color component and a gray component, which will make the application of our image processing method more convenient in HSI color space [17,18]. The conversion from RGB color space to HSI color space can be achieved by using the following formulas. The hue component is calculated as:

$$H = \begin{cases} \theta, & B \le G \\ 360 - \theta, & B > G, \end{cases} \tag{2}$$

where

$$\theta = \arccos\left\{ \frac{1/2[(R-G)+(R-B)]}{[(R-G)^2+(R-G)(G-B)]^{1/2}} \right\}, \tag{3}$$

The saturation component is given as:

$$S = 1 - \frac{3}{R+G+B}[\min(R,G,B)], \tag{4}$$

Finally, the intensity component is given by:

$$I = \frac{1}{3}(R+G+B), \tag{5}$$

3. Dehazing method

By comparing and analyzing the image dehazing experimental results for the H, S, and I components, we

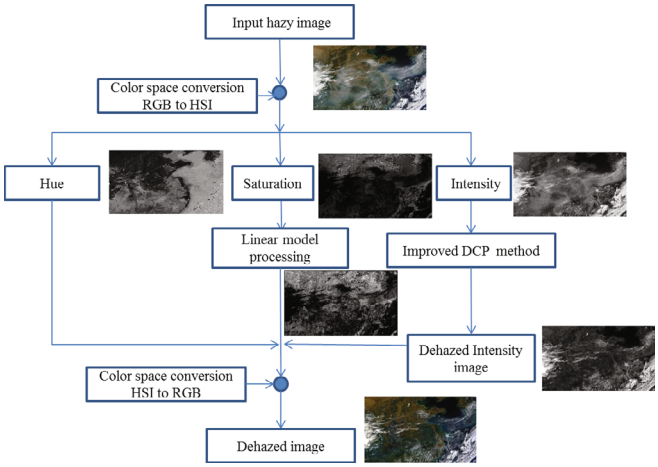

Fig. 2. (Color online) Overall flowchart of the proposed method.

found that the saturation component and the brightness component were positively correlated with the concentration of haze, and that the H component undergoes no obvious change before and after haze removal processing. And the results are shown in Fig. 1.

Therefore, a hazy image is transformed from RGB color space into HSI color space for image processing, and the intensity and the saturation components are processed while the hue component remains unchanged. The overall flowchart of the proposed method is shown in Fig. 2.

For a haze-free image, the saturation value of each pixel is relatively large. Because of the existence of fog, the saturation of atmospheric light is introduced, resulting in the dilution of saturation. Thus, we established a linear model to estimate the saturation $S\left(x,y\right)$ component:

$$S\left(x,y\right)=\theta_0+\theta_1 S_1\left(x,y\right)+\theta_2 S_A\left(x,y\right), \tag{6}$$

where θ_i, i $\in (0,1,2)$, represents nonnegative coefficients, $S_1\left(x,y\right)$ is the saturation of a hazy image, and $S_A\left(x,y\right)$ represents the saturation of atmospheric light. The gradient descent method is applied to learn θ_i, and a cost function $J\left(\theta_i\right)$ is introduced, which is the sum of squares of all modeling error, $J(\theta_i)$ can be described using:

$$J(\theta)=\frac{1}{2m}\sum_{i=1}^{m}\left(S_\theta(X^i)-y^i\right)^2, \tag{7}$$

where m is the total number of training samples and y^i is the actual value of the samples.

We can obtain the coefficients by minimizing the cost function. At first, we randomly select a combination of parameters $(\theta_0,\theta_1,\theta_2)$ to calculate the cost function; then, we look for the next combination of parameters to make the value drop most until the cost function reaches a local minimum. The derivative of the cost function is calculated as

$$\frac{\partial}{\partial\theta_j}J(\theta)=\frac{\partial}{\partial\theta_j}-\frac{1}{2m}\sum_{i=1}^{m}\left(S_\theta(X^i)-y^i\right)^2, \tag{8}$$

According to the gradient descent algorithm we have

$$\theta_j:=\theta_j-\alpha\frac{\partial}{\partial\theta_j}J(\theta), \tag{9}$$

θ is updated during gradient descent, so we have the following expressions:

$$\theta_0:=\theta_0-\alpha\frac{1}{m}\sum_{i=1}^{m}(S_\theta(X^i)-y^i), \tag{10}$$

$$\theta_1:=\theta_1-\alpha 1/m\sum_{i=1}^{m}S_\theta((X^i)-y^i)X_1^{(i)}, \tag{11}$$

$$\theta_2:=\theta_2-\alpha 1/m\sum_{i=1}^{m}S_\theta((X^i)-y^i)X_2^{(i)}, \tag{12}$$

where the notation := represents that the set of the values of θ_j ion the left side of the equation is equal to the set of the value on the right side, and α is the learning rate, which determines the efficiency of the gradient descent algorithm. If the learning rate is too small, a large number of steps will be needed to reach the global minimum. Conversely, if the learning rate is too large, the cost function will not converge. Thus, choose the right learning rate is crucial.

The learning rate can be calculate using

$$\alpha=\alpha_S*\alpha_D^{\frac{\mathrm{global-step}}{\mathrm{decay-step}}}, \tag{13}$$

where α_S is the initial learning rate, α_D indicates the attenuation rate of each round of learning, $\mathrm{global}-\mathrm{step}$ represents the current number of learning steps which is equivalent to how many times we have put batch into the learner, and $\mathrm{decay}-\mathrm{step}$ is the number of steps per round of learning which is equal to the total number of samples divided by the size of each batch. Then the saturation of atmospheric light S_A is estimated. Owing to atmospheric light corresponds to the most dense haze area, so the 1/4 brightest region in the image is selected, and the minimum pixel value in the region is used as an estimate of S_A.

We implement the improved DCP method [14] in the intensity channel. We obtain the transmission $t(x)$ based on the DCP theory. Then, the atmospheric light estimation method of He *et al.* is improved. In He *et al.*'s work [14], the top 0.1% of pixels in the dark channel are taken as the atmospheric light. Although this method is robust, only one point is taken into account which maybe the reason that the **A** value of each channel is too high to result in color drift. Achieving satisfactory results with conventional methods is difficult when highlight areas exist in the image.

$$M(x)=\min_{c\in(r,g,b)}(I_c(x)). \tag{14}$$

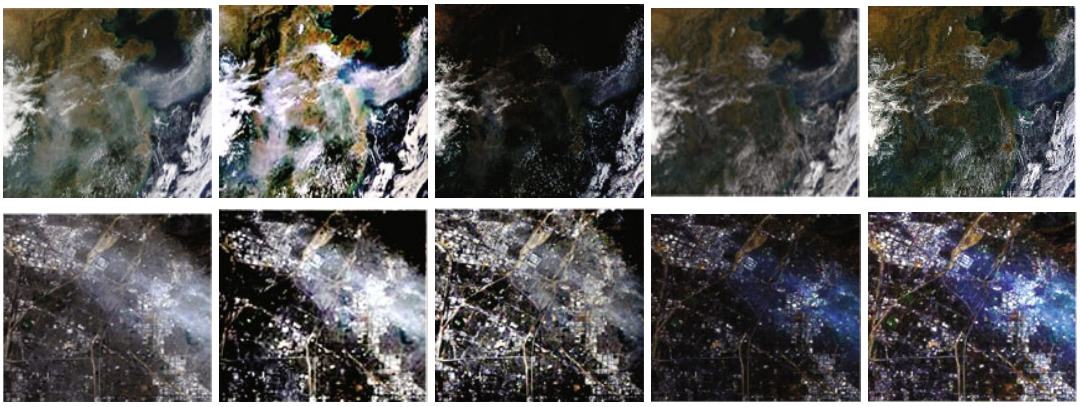

(a) (b) (c) (d) (e)

Fig. 3. (Color online) Qualitative comparison of different methods: (a) hazy images, (b) MSR method results, (c) Tan's method results, (d) DCP method results, and (e) our results.

Based on the work of He and others, we developed a method that can reduce the influence of highlight areas on the acquisition of atmospheric light. First, it's required a minimum channel map of the degraded remote sensing images. The minimum channel map can be calculated as follows:

$$\text{score}_i = \bar{M}_i - \delta_i^2, \quad i = 1, 2, \tag{15}$$

where i is the index of each region, $score_i$ is the score of region i, M_i represents the mean value of the region i and δ_i^2 represents the variance in the region i. Then, the region with the highest score is taken as the candidate iterative region and is further divided into four smaller regions. The process continues until the size of the candidate region is smaller than the preset size threshold. The average of each channel in the last candidate region is selected as the result of $\mathbf{A}$. Thus, we can obtain the haze-free intensity component image $\mathbf{I}(x)$ because we have estimates of $\mathbf{A}$ and $t(x)$:

$$\mathbf{I}(x) = \frac{\mathbf{I}(x) - \mathbf{A}}{t(x)} + \mathbf{A}. \tag{16}$$

Finally, these three channel images are transformed from HSI color space back to RGB color space.

III. EXPERIMENT

To validate the effectiveness of the method, we tested multiple remote sensing hazy images. The images used in this research were collected from the NASA Earth Observatory website and the Earth Explorer of the United States Geological Survey (USGS). The performance of the proposed method is compared with that of the Multiscale Retinex method [12], the Tan's method [13] and the DCP method [14] are both qualitative and quantitative. In order to verify the improvement of in image visual effect for each algorithm, we selected typical images to processed, as shown in Fig. 3.

Figures 3(a) and 3(b) show an input hazy image and the multi-scale Retinex method results respectively. Although the MSR algorithm has good performance in contrast enhancement, it will lead to color distortion when the original image does not satisfy the gray assumption. Figure 3(c) show Tan's method results, in which most of the haze has been removed, but the recovered image has a slight color distortion, and the resolution of the image is lower than the original image. Figure 3(d) presents the DCP method result, which is constrained by the inherent problem of dark channel priors; He *et al.*'s algorithm cannot be applied to areas in which the brightness in the region is similar to that of atmospheric light. Therefore, the DCP method is often unreliable when dealing with non-homogeneous images. Figure 3(e) presents our method's results; as can be seen, the dense haze is effectively removed, and color fidelity is preserved. Our method achieves a better result.

1. Quantitative results comparison

In order to quantitatively evaluate the algorithms, we select some classical evaluation indices, including the mean squared error (MSE), the structural similarity (SSIM), the ratio of new visible edges (e), the gain of visibility level $\bar{r}$ and the fog aware density evaluator (FADE). Structural similarity (SSIM) is an objective evaluation index that is independent of the brightness and the contrast of the image and conforms to the characteristics of the human visual system. A high SSIM value indicates that the image with haze removed is very similar to the real image on the ground [19].

By comparing the processing results of each algorithm, we concluded that the SSIM value obtained by this method is higher; the results are shown in Table 1. The

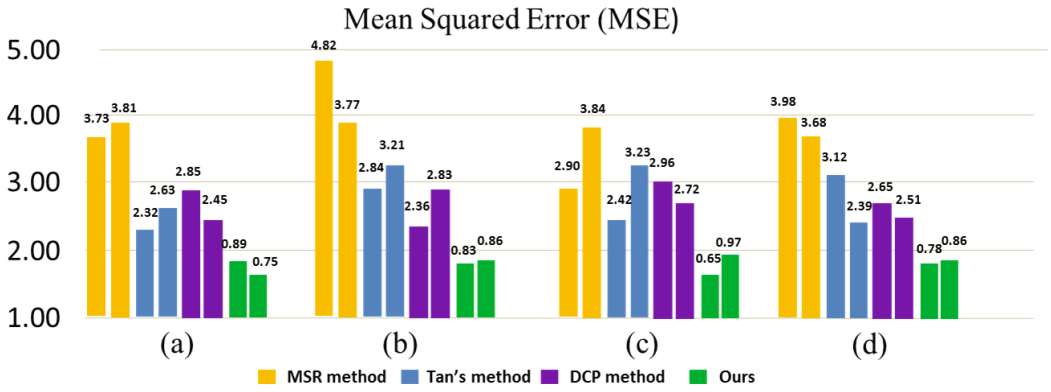

Fig. 4. (Color online) The corresponding MSE calculation results.

Table 1. The values of SSIM, e, $\bar{r}$ and FADE

Image	SSIM	e	$\bar{r}$	FADE
Original	0.737	2.627	2.315	0.348
	0.685	0.668	2.168	0.606
MSRCR method	0.774	2.806	1.785	0.269
	0.732	0.927	1.654	0.472
Tan's method	0.763	2.763	1.646	0.335
	0.742	0.664	1.235	0.616
DCP method	0.712	2.782	1.836	0.317
	0.746	0.757	1.757	0.608
Our method	0.739	2.798	1.963	0.305
	0.7216	0.786	1.935	0.496

MSE can be utilized as a more convenient way to evaluate the degree of data variation [20,21]. A high value of MSE indicates that the haze-removal algorithm is not effective while a low value of MSE indicates that the recovered image is valuable. The value of e evaluates the ability of the haze-removal method to recover the edges that are not visible in a hazy image. The value of $\bar{r}$ represents the average ratio of gradient specifications before and after dehazing [22]. The Fog Aware Density Evaluator [23] (FADE) is a contrast descriptor that indicates the visibility of a foggy scene by measuring the statistical regularity deviation of hazy images and haze-free images. A low value of the FADE implies better visibility enhancement. We show the corresponding MSE results produced by the different algorithms in Fig. 4, we list the values of SSIM, e, $\bar{r}$ and FADE in Table 1.

To sum up, our method achieves the smallest values of MSE and FADE, the highest value of SSIM, e and $\bar{r}$. Therefore, the results of these experimental data indicate that our algorithm achieves better performance in contrast enhancement, image structure information preservation, visible edge enhancement, and haze removal. As a consequence, the proposed method in this research is valuable for haze removal.

IV. CONCLUSION

We have developed a novel and effective dehazing algorithm to achieve single remote-sensing image dehazing. A linear regression model is proposed to estimate the saturation component; and the gradient descent method is applied to learn the coefficients of the linear model. In addition, we improved the DCP method by proposing a new method to estimate the atmospheric light, which can limit the influence of highlight areas. Compared with the traditional haze-removal methods, the experimental results demonstrate that the developed algorithm performs better. Both qualitative evaluations and quantitative assessments indicate that the proposed method can recover a haze-free remote-sensing image with good visual effect and high quality. The following research will be aimed at dealing with dense haze.

ACKNOWLEDGMENTS

This work is partially supported by the National Key R&D Program of China (Grants No. 2016YFB0500100).

REFERENCES

[1] M. Qin, F. Xie and W. Li, J. IEEE J. Select. Top. Appl. Earth Observations & Remote Sensing. **11**, 99 (2018).
[2] L. Jiao, Z. Shi and W. Tang, J. Int. Conf. Comp. Vision Remote Sensing IEEE. **52**, 132 (2013).
[3] S. Liang, H. Fang and M. Chen, J. IEEE Trans. Geosc. Remote Sensing **39**, 2490 (2001).
[4] Q. Liu, X. Gao, L. He and W. Lu, J. Signal Process **137**, 33 (2017).
[5] X. C. Yu *et al.*, J. Light Sci. Appl. **7**, 18003 (2018).
[6] Y. C Wu *et al.*, J. Light Sci. Appl. **6**, 46 (2017).
[7] C. Han and C. C. Chung, J. Korean Phys. Soc. **60**, 680 (2012).
[8] H. Jeon, H. Youn and Nam, J. Korean Phys. Soc. **72**, 539 (2018).

[9] T. K. Kim, J. K. Paik and B. S. Kang, J. IEEE Trans. Consumer Electron. **44**, 82 (1998).
[10] M. J. Seow and V. K. Asari, J. Neurocomputing. **69**, 954 (2006).
[11] E. H. Land, J. Proc. Natl. Acad. Sci. USA. **80**, 5163 (1983).
[12] R. Kimmel, M. Elad and D. Shaked, Int. J. Comput. Vision **52**, 7 (2003).
[13] R. T. Tan, in *26th IEEE Conference on Computer Vision and Pattern Recognition, CVPR* (2008), Vol. 8, p. 1.
[14] K. M. He, J. Sun and X. Tang, J. IEEE Trans. Pattern Anal. Mach. Intell. **33**, 2341 (2011).
[15] S. K. Nayar and S. G. Narasimhan, in *Proceedings of the Seventh IEEE International Conference on Computer Vision* (IEEE Comput. Soc., 1999).
[16] C. Connolly and T. Fleiss, J. IEEE Trans Image Process **6**, 1046 (1997).
[17] Narasimhan, G. Srinivasa and S. K. Nayar, J. Int. Comput. Vision **48**, 233 (2002).
[18] B. V. Dhandra, R. Hegadi, M. Hangarge and V. S. Malemath, *Int. Conf. Pattern Recognition* (IEEE Comput. Soc., 2006).
[19] W. Zhang, J. Liang and L. Ren, J. Optics **19**, 9 (2017).
[20] Z. Wang and A. C. Bovik, Synthesis Lectures on Image Video & Multimedia Process **2**, 156 (2006).
[21] Q. S. Zhu, J. Mai and L. Shao, J. IEEE Trans. Image Process **24**, 3522 (2015).
[22] E. Peli, J. Opt. Soc. Am. Optics Image Sci. & Vision **7**, 2032 (1990).
[23] L. K. Choi, J. You and A. C. Bovik, J. IEEE Trans. Image Process **24**, 3888 (2015).